JACS
JOURNAL OF THE AMERICAN CHEMICAL SOCIETY

Communication

Oxygen Activation by Co(II) and a Redox Non-Innocent Ligand: Spectroscopic Characterization of a Radical–Co(II)–Superoxide Complex with Divergent Catalytic Reactivity

Amanda R. Corcos, Omar Villanueva, Richard C. Walroth, Savita K. Sharma, John Bacsa, Kyle M. Lancaster, Cora E. MacBeth, and John F. Berry

J. Am. Chem. Soc., **Just Accepted Manuscript** • DOI: 10.1021/jacs.5b12643 • Publication Date (Web): 22 Jan 2016

ACS Publications

Journal of the American Chemical Society is published by the American Chemical Society. 1155 Sixteenth Street N.W., Washington, DC 20036

that each $(L)^{3-}$ ligand coordinates to a single Co center in a novel tridentate pincer-like coordination mode.[6]

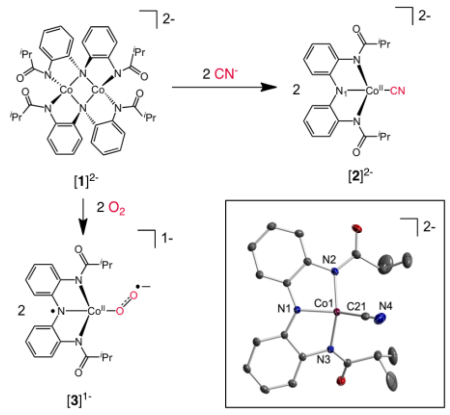

Figure 1. Preparation of $[\mathbf{2}]^{2-}$ and $[\mathbf{3}]^{1-}$ from $[\mathbf{1}]^{2-}$. Thermal ellipsoid plot of $[\mathbf{2}]^{2-}$ is shown at the 45% probability level, with H atoms and counter cations omitted for clarity.

Several spectroscopic techniques were employed to determine the first observable catalytically-relevant intermediate responsible for the divergent reactivity of $[\mathbf{1}]^{2-}$. Gas-uptake experiments indicate that $[\mathbf{1}]^{2-}$ reacts with O_2 in a 1:2 stoichiometry (see SI), suggesting that one molecule of O_2 is taken up per Co center. UV-Vis spectroscopy shows isosbestic behavior, indicating clean conversion of $[\mathbf{1}]^{2-}$ to $[\mathbf{3}]^{1-}$ via a short-lived intermediate (Figure S4). The resulting burgundy species $[\mathbf{3}]^{1-}$ can be isolated or used in-situ to perform stoichiometric oxidations with PPh_3 and 2-PPA, generating the same products of catalytic oxidations using $[\mathbf{1}]^{2-}$ (see SI). Along with the monometallic structure of $(Et_4N)_2[\mathbf{2}]$, this result suggests that $[\mathbf{1}]^{2-}$ reacts with O_2 to form a monometallic Co–O_2 species, $[Co(L)O_2]^{1-}$, $[\mathbf{3}]^{1-}$. The monomeric nature of $[\mathbf{3}]^{1-}$ is further supported by MALDI-TOF mass spectrometry, which shows that new ions with m/z = 410.49 or 412.47 amu are produced when $[\mathbf{1}]^{2-}$ reacts with 2 equivalents of $^{16}O_2$ or $^{18}O_2$, respectively (Figure S5). These mass values are consistent with formulations as $[\mathbf{3} - {}^{16/18}O]^-$ species, similar to mass spectral data observed for a recently reported five-coordinate Co–O_2 complex capable of C–H bond activation via a postulated Co^{IV}-oxo intermediate.[12] Liquid-cell IR techniques show that $[\mathbf{3}]^{1-}$ has an O_2 stretching feature at 1248 cm^{-1}, which shifts to 1203 cm^{-1} upon $^{18}O_2$ labeling (Figure S6). These data are consistent with end-on Co–superoxide coordination.[13]

This molecular geometry is further supported by analysis of extended X-ray absorption fine structure (EXAFS) in the Co K-edge XAS of $[\mathbf{2}]^{2-}$ and $[\mathbf{3}]^{1-}$ (Figures S7-8, Table S1). The EXAFS of $[\mathbf{2}]^{2-}$ and $[\mathbf{3}]^{1-}$ are qualitatively similar, yielding a Co coordination number of four with average Co–L distances of 1.98 Å and 1.88 Å, respectively. These distances are in good agreement with the crystallographic and DFT-optimized average Co–L distances of 2.01 Å and 2.04 Å for $[\mathbf{2}]^{2-}$, respectively, and are also in good agreement with the calculated average Co–L distance for $[\mathbf{3}]^{1-}$ at 1.87 Å. These results suggest a similar coordination geometry for $(L)^{3-}$ in $[\mathbf{2}]^{2-}$ and $[\mathbf{3}]^{1-}$, further indicating a monomeric Co(L) end-on superoxide structural unit for $[\mathbf{3}]^{1-}$.

Ground state electronic configurations of $[\mathbf{2}]^{2-}$ and $[\mathbf{3}]^{1-}$ were established from their magnetic properties. For $[\mathbf{2}]^{2-}$, the μ_{eff} value of 4.27(3) μ_B at 298K in $CDCl_3$ is indicative of an S = 3/2 ground state. EPR data (Figure 2a) confirm this unusual high-spin state, with observed (effective) g values of g_x = 4.53, g_y = 3.97, and g_z = 1.95, indicating $D > h\nu$. Despite the clear indication of an S = 3/2 ground state for $[\mathbf{2}]^{2-}$, the EPR spectrum for $[\mathbf{3}]^{1-}$ is surprisingly characteristic of an S = 1/2 species, best simulated by g_x = 2.20, g_y = 2.00, g_z = 1.975 (μ_{eff} = 2.13 μ_B at 298K in CH_3CN). The observation of a "high-spin" complex of cyanide, a strong-field ligand, is unusual[14] but consistent with the low coordination number. Even more unusual is that the weaker field O_2^- complex, $[\mathbf{3}]^{1-}$, appears low spin. Co Kβ X-ray emission spectra (XES) of $[\mathbf{2}]^{2-}$ and $[\mathbf{3}]^{1-}$ were measured as a probe of the local spin at Co (Figure 2b). Splitting of Kβ (3p→1s) main lines into Kβ′ and $K\beta_{1,3}$ features is a useful metric of spin population since electron delocalization out of metal 3d orbitals results in attenuation of the 3d–3p exchange energy.[15] Kβ main line splitting is markedly decreased in $[\mathbf{3}]^{1-}$ compared to $[\mathbf{1}]^{2-}$ and $[\mathbf{2}]^{2-}$, consistent with a decreased local Co spin population in $[\mathbf{3}]^{1-}$.

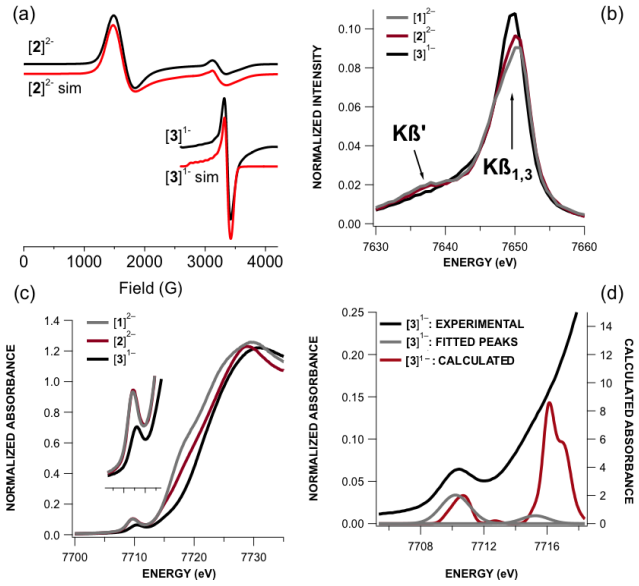

Figure 2. (a) Experimental EPR data and simulations for $[\mathbf{2}]^{2-}$ and $[\mathbf{3}]^{1-}$. (b) Co Kβ XES main lines of $[\mathbf{1}]^{2-}$–$[\mathbf{3}]^{1-}$. (c) Co K-edge XANES of $[\mathbf{1}]^{2-}$–$[\mathbf{3}]^{1-}$. Inset: Magnification of the Co 1s → (Co 3d + L) pre-edge features. (d) Overlay of calibrated TDDFT-calculated (B3LYP/def2-TZVP-ZORA) Co K-edge XANES pre-edge peaks for $[\mathbf{3}]^{1-}$.

To defuse this spin state conundrum, DFT calculations were employed to produce an electronic structure picture consistent with the aggregate structural and spectral data.

To this end, we evaluated multiple electronic configurations for $[\mathbf{2}]^{2-}$ and $[\mathbf{3}]^{1-}$.[16] The quartet state for $[\mathbf{2}]^{2-}$ was energetically favored over the doublet state by 26.7 kJ/mol, in agreement with the EPR data and the similarity of the Co XANES pre-edge energy of $[\mathbf{2}]^{2-}$ with that of $[\mathbf{1}]^{2-}$, for the Co^{II} centers in $[\mathbf{1}]^{2-}$ are high-spin[6] (Figure 2c). The optimized geometry for $[\mathbf{2}]^{2-}$ as a quartet is also a superior match to the crystallographic data (Table S5). Additionally, the cyanide C≡N stretch predicted to occur at 2211 cm^{-1} is experimentally measured at 2109 cm^{-1}, in decent agreement given the well-known tendency for DFT to overestimate vibrational frequencies.[17]

For $[\mathbf{3}]^{1-}$, calculations support an S = 1/2 end-on superoxide species as the configuration with lowest energy (Table S6),[18] in accord with experimental data. For this species, a spin-coupled electronic structure is obtained. There are two low-lying doubly-occupied Co-centered *e*-type orbitals of the pseudotetrahedral Co *d* orbital manifold and three singly-occupied orbitals for the t_2-derived set (Figure 3, S13). The superoxide ligand has two π* valence orbitals—doubly-occupied π_1* and singly-occupied π_2*—that interact with the Co t_2-derived orbitals. The π_1* orbital engages in a 3-electron σ interaction with one Co orbital, while the π_2* unpaired electron is coupled with another Co electron. A second antiferromagnetic interaction exists between the third Co t_2-derived electron and a ligand-based orbital having significant character from the central N atom of L. Therefore, as with $[\mathbf{2}]^{2-}$, the metal center in $[\mathbf{3}]^{1-}$ contains a high-spin S = 3/2 Co^{II} center. In this case, however, two of the three unpaired electrons of the Co^{II} center couple with an L radical and a superoxide radical to yield an overall S = 1/2 ground state. This electronic structure explains the divergent reactivity of $(Et_4N)[\mathbf{3}]$ (*vide supra*), for the half-filled O_2 π_2* orbital can be either a donor orbital for nucleophilic reactivity or an acceptor orbital for electrophilic reactivity.

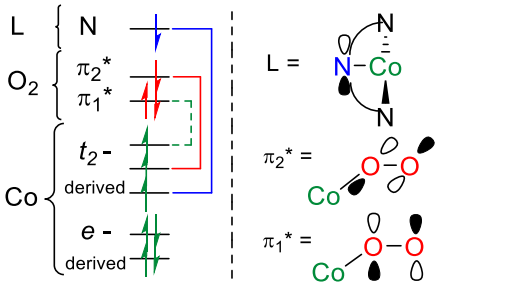

Figure 3. Molecular orbital interactions for $[\mathbf{3}]^{1-}$. (left) Green, red, and blue arrows represent electrons in Co-, O_2-, and ligand-based orbitals, respectively. The red and blue brackets show antiferromagnetic coupling between the O_2- and N-based ligands with Co d electrons. The green dashed bracket shows the 3-electron σ interaction between a Co electron and the π_1* of the O_2^- ligand. (right) Representation of ligand- and O_2-based orbitals.

The Co K-edge XANES of $[\mathbf{1}]^{2-}$–$[\mathbf{3}]^{1-}$ (Figure 2c) deserve further comment. All of the other experimental and computational data clearly indicate that the Co^{II} oxidation state remains constant throughout this series, but the pre-edge features in the spectra of $(Et_4N)_2[\mathbf{1}]$ and $(Et_4N)_2[\mathbf{2}]$ effectively superimpose at 7709.7 eV, while that for $[\mathbf{3}]^{1-}$ is shifted in energy to 7710.2 eV. Furthermore, rising edges distinguish all three compounds (Figure S9).

TD-DFT analysis of XANES pre-edge features, accomplished via calibration to a set of model compounds (Figure S10), was performed to reconcile the XANES features with the electronic structures of $[\mathbf{1}]^{2-}$–$[\mathbf{3}]^{1-}$. For $[\mathbf{2}]^{2-}$, this led to a straightforward assignment of the pre-edge transition as arising from the Co 1s to the valence "t_2"-derived set. In the case of $[\mathbf{3}]^{1-}$ (Figure 2d), the acceptor orbitals participating in this excitation have substantial O–O π* admixture. Comparison of the spin density plots of $[\mathbf{2}]^{2-}$ vs $[\mathbf{3}]^{1-}$ shows this effect quite clearly; while the spin density in $[\mathbf{2}]^{2-}$ is highly localized on the metal center with orbitals having roughly 70% metal character, the spin for $[\mathbf{3}]^{1-}$ is more delocalized and the orbitals are closer to 50% metal in character (Figure S11).

This delocalization of electron density manifests in the calculated Co atomic charges 0.47, 0.55, and 0.64 for $[\mathbf{1}]^{2-}$, $[\mathbf{2}]^{2-}$, and $[\mathbf{3}]^{1-}$, respectively. These values correlate to a reasonable degree (R^2 = 0.94) with the corresponding rising edge inflection points (Figure S9). Moreover, the trend line extrapolates to 7706 ± 3 eV at a charge of 0, consistent with the rising edge inflection of Co metal (7709 eV). Consequently, variations in the XANES of $[\mathbf{3}]^{1-}$ from the other compounds do not necessarily reflect a change in the physical oxidation state at Co after reaction with O_2. The difference in energy of the Co K-edge XANES pre-edge features is due to a difference in the nature of the acceptor orbital when comparing $[\mathbf{1}]^{2-}$ and $[\mathbf{2}]^{2-}$ to $[\mathbf{3}]^{1-}$, as has been seen previously for Cu complexes.[19] The shift to higher energy of the rising edge inflection point in $[\mathbf{3}]^{1-}$ likely reflects the highly covalent interaction of Co with an electronegative O-donor. Although XANES is widely used as a metric of physical oxidation states of transition metal complexes, we emphasize here that the nature of the coordinated ligands also has a strong influence over the spectral profiles.

In summary, the reaction of $[\mathbf{1}]^{2-}$ with 2 equivalents of $[Et_4N]CN$ yields the unusual, high-spin Co^{II} complex $[\mathbf{2}]^{2-}$, which provides structural insight toward the catalytically relevant intermediate $[\mathbf{3}]^{1-}$. Compound $[\mathbf{3}]^{1-}$ is determined to be a monomeric Co^{II} superoxide complex supported by the redox non-innocent ligand L in its singly-oxidized radical form. The local spin state of Co^{II} is S = 3/2, but these electrons couple with unpaired electrons on L as well as the O_2^- ligand to yield an overall S = 1/2 state, as seen via EPR spectroscopy. The catalytic utility of $[\mathbf{3}]^{1-}$ is therefore attributable to its redox non-innocent L supporting ligand, allowing Co to remain high-spin upon activation of O_2 and avoiding the kinetic quagmire that is a low-spin Co^{III} complex.

ASSOCIATED CONTENT

Synthetic and spectroscopic methods, full MO diagrams, Cartesian coordinates, and CIF for $[\mathbf{2}]^{2-}$. This material is available free of charge via the Internet at http://pubs.acs.org.

AUTHOR INFORMATION

Corresponding Authors

* berry@chem.wisc.edu
* cora.macbeth@emory.edu
* kml236@cornell.edu

Present Address

∇ Department of Natural Sciences, Dalton State College

Notes

The authors declare no competing financial interest.

ACKNOWLEDGMENT

We thank NSF for support (CHE-1205646). J.F.B. thanks the DOE (DE-FG02-10ER16204). K.M.L thanks Cornell University for startup funding and NSF (CHE-1454455). A.R.C. thanks the NSF (DGE-0718123). R.C.W. thanks the NIH-NIGMS (T32GM008500). Computational (CHE-0840494) and EPR facilities (CHE-0741901) at UW-Madison are supported by NSF. We thank Dr. Elizabeth Blaesi for insightful discussions. This work is based on research conducted at the Cornell High Energy Synchrotron Source (CHESS), supported by NSF and NIH/NIGMS under NSF award DMR-1332208.

REFERENCES

1. (a) Werner, A.; Mylius, A. *Z. Anorg. Chem.* **1898**, *16* (1), 245-267; (b) Tsumaki, T. *Bull. Chem. Soc. Jpn.* **1938**, *13* (2), 252-260.
2. (a) Schaefer, W. P.; Marsh, R. E. *J. Am. Chem. Soc.* **1966**, *88* (1), 178-179; (b) Floriani, C.; Calderazzo, F. *J. Chem. Soc. A* **1969**, (6), 946-953; (c) Rodley, G. A.; Robinson, W. T. *Nature* **1972**, *235* (5339), 438-439; (d) Fritch, J. R.; Christoph, G. G.; Schaefer, W. P. *Inorg. Chem.* **1973**, *12* (9), 2170-2175; (e) Collman, J. P.; Gagne, R. R.; Kouba, J.; Ljusberg-Wahren, H. *J. Am. Chem. Soc.* **1974**, *96* (21), 6800-6802; (f) Gall, R. S.; Rogers, J. F.; Schaefer, W. P.; Christoph, G. G. *J. Am. Chem. Soc.* **1976**, *98* (17), 5135-5144; (g) James, B. R. "Interaction of Dioxygen with Metalloporphyrins" In *The Porphyrins*. Dolphin, D., Ed. Academic Press: New York, 1979; Vol. 5, pp 207-215; (h) Jones, R. D.; Summerville, D. A.; Basolo, F. *Chem. Rev.* **1979**, *79* (2), 139-179; (i) Bailey, C. L.; Drago, R. S. *Coord. Chem. Rev.* **1987**, *79* (3), 321-332; (j) Busch, D. H.; Alcock, N. W. *Chem. Rev.* **1994**, *94* (3), 585-623; (k) Hikichi, S.; Akita, M.; Moro-oka, Y. *Coord. Chem. Rev.* **2000**, *198* (1), 61-87; (l) Cho, J.-H.; Sarangi, R.; Kang, H.-Y.; Lee, J.-Y.; Kubo, M.; Ogura, T.; Solomon, E. I.; Nam, W.-W. *J. Am. Chem. Soc.* **2010**, *132* (47), 16977-16986; (m) Tiné, M. R. *Coord. Chem. Rev.* **2012**, *256* (1-2), 316-327.
3. (a) Smith, T. D.; Pilbrow, J. R. *Coord. Chem. Rev.* **1981**, *39* (3), 295-383; (b) Mandal, A. K.; Iqbal, J. *Tetrahedron* **1997**, *53* (22), 7641-7648; (c) Sharma, V. B.; Jain, S. L.; Sain, B. *Tetrahedron Lett.* **2003**, *44* (2), 383-386; (d) Schultz, M. J.; Sigman, M. S. *Tetrahedron* **2006**, *62* (35), 8227-8241.
4. (a) Merkx, M.; Kopp, D. A.; Sazinsky, M. H.; Blazyk, J. L.; Müller, J.; Lippard, S. J. *Angew. Chem. Int. Ed.* **2001**, *40* (15), 2782-2807; (b) Solomon, E. I.; Heppner, D. E.; Johnston, E. M.; Ginsbach, J. W.; Cirera, J.; Qayyum, M.; Kieber-Emmons, M. T.; Kjaergaard, C. H.; Hadt, R. G.; Tian, L. *Chem. Rev.* **2014**, *114* (7), 3659-3853; (c) Wang, W.; Liang, A. D.; Lippard, S. J. *Acc. Chem. Res.* **2015**, *48* (9), 2632-2639.
5. (a) Jazdzewski, B. A.; Tolman, W. B. *Coord. Chem. Rev.* **2000**, *200-202*, 633-685; (b) Meunier, B.; de Visser, S. l. P.; Shaik, S. *Chem. Rev.* **2004**, *104* (9), 3947-3980; (c) Denisov, I. G.; Makris, T. M.; Sligar, S. G.; Schlichting, I. *Chem. Rev.* **2005**, *105* (6), 2253-2278; (d) *Cytochrome P450: Structure, Mechanism, and Biochemistry*. 3rd ed.; Ortiz de Montellano, P. R. Kluwer/Plenum: New York, 2005; (e) Rose, E.; Andrioletti, B.; Zrig, S.; Quelquejeu-Etheve, M. *Chem. Soc. Rev.* **2005**, *34* (7), 573-583; (f) Chirik, P. J.; Wieghardt, K. *Science* **2010**, *327* (5967), 794-795.
6. Sharma, S. K.; May, P. S.; Jones, M. B.; Lense, S.; Hardcastle, K. I.; MacBeth, C. E. *Chem. Commun.* **2011**, *47* (6), 1827-1829.
7. Patra, T.; Manna, S.; Maiti, D. *Angew. Chem. Int. Ed.* **2011**, *50* (51), 12140-12142.
8. For examples of M-O_2 complexes that require hydrogen peroxide and excess base to perform stoichiometric deformylation, see: (a) Seo, M. S.; Kim, J. Y.; Annaraj, J.; Kim, Y.; Lee, Y.-M.; Kim, S.-J.; Kim, J.; Nam, W. *Angew. Chem., Int. Ed.* **2007**, *46* (3), 377-380; (b) Jo, Y.; Annaraj, J.; Seo, M. S.; Lee, Y.-M.; Kim, S. Y.; Cho, J.; Nam, W. *J. Inorg. Biochem.* **2008**, *102* (12), 2155-2159; (c) Cho, J.; Sarangi, R.; Nam, W. *Acc. Chem. Res.* **2012**, *45* (8), 1321-1330; (d) Cho, J.; Kang, H. Y.; Liu, L. V.; Sarangi, R.; Solomon, E. I.; Nam, W. *Chem. Sci.* **2013**, *4* (4), 1502-1508; (e) Shokri, A.; Que, L. *J. Am. Chem. Soc.* **2015**, *137* (24), 7686-7691.
9. For a Cu^{II}-superoxide complex that is capable of stoichiometric deformylation but requires superoxide, not O_2, see: (a) Donoghue, P. J.; Gupta, A. K.; Boyce, D. W.; Cramer, C. J.; Tolman, W. B. *J. Am. Chem. Soc.* **2010**, *132* (45), 15869-15871; (b) Pirovano, P.; Magherusan, A. M.; McGlynn, C.; Ure, A.; Lynes, A.; McDonald, A. R. *Angew. Chem. Int. Ed.* **2014**, *53* (23), 5946-5950; (c) Ure, A. D.; McDonald, A. R. *Synlett* **2015**, *26* (15), 2060-2066.
10. Classification of reactive metal-oxygen species as electrophilic implies reactivity such as O-atom transfer, hydrogen atom abstraction, and electron transfer. Nucleophilic metal-oxygen species react with electron deficient substrates such as 2-PPA to produce acetophenone.
11. The τ_δ value distinguishes between "pinched" tetrahedral and sawhorse geometries. τ_δ values close to 1.0 indicate tetrahedral geometry, while τ_δ values between 0.45–0.63 are best described as distorted sawhorse geometries. See: Reineke, M. H.; Sampson, M. D.; Rheingold, A. L.; Kubiak, C. P. *Inorg. Chem.* **2015**, *54* (7), 3211-3217.
12. Nguyen, A. I.; Hadt, R. G.; Solomon, E. I.; Tilley, T. D. *Chem. Sci.* **2014**, *5* (7), 2874-2878.
13. Nakamoto, K. *Infrared and Raman Spectra of Inorganic and Coordination Compounds. Part B: Applications in Coordination, Organometallic, and Bioinorganic Chemistry*. Wiley: New York, 1997.
14. (a) Nelson, K. J.; Giles, I. D.; Shum, W. W.; Arif, A. M.; Miller, J. S. *Angew. Chem. Int. Ed.* **2005**, *44* (20), 3129-3132; (b) Scott, T. A.; Berlinguette, C. P.; Holm, R. H.; Zhou, H.-C. *Proc. Natl. Acad. Sci. U.S.A.* **2005**, *102* (28), 9741-9744.
15. Pollock, C. J.; Delgado-Jaime, M. U.; Atanasov, M.; Neese, F.; DeBeer, S. *J. Am. Chem.Soc.* **2014**, *136* (26), 9453-9463.
16. For calculations ruling out a possible Co^{III}-peroxide assignment for $[\mathbf{3}]^{1-}$, see SI .
17. Hehre, W. J. R., L.; Schleyer, P. V. R.; Pople, J. A. *Ab Initio Molecular Orbital Theory*. Wiley: New York, 1986.
18. The ground state of $[\mathbf{3}]^{1-}$ was also assessed with SORCI calculcations (see SI).
19. (a) Tomson, N. C.; Williams, K. D.; Dai, X.; Sproules, S.; DeBeer, S.; Warren, T. H.; Wieghardt, K. *Chem. Sci.* **2015**, *6* (4), 2474-2487; (b) Walroth, R. C.; Uebler, J. W. H.; Lancaster, K. M. *Chem. Commun.* **2015**, *51*, 9864-9867.

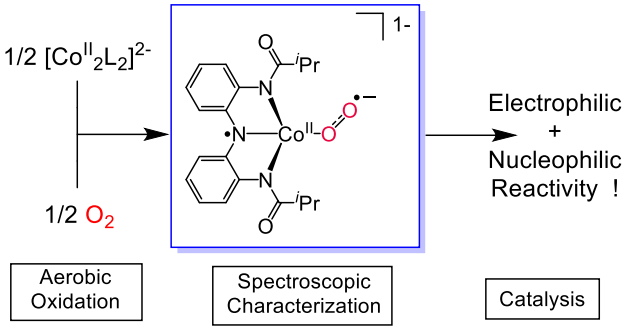
1/2 [Co$^{II}_2$L$_2$]$^{2-}$
1/2 O_2
1-
Co^{II}-O
Electrophilic
+
Nucleophilic
Reactivity !
Aerobic Oxidation
Spectroscopic Characterization
Catalysis